The not-so-simple effects of boundary conditions on models of simple shear

Marcel Frehner[1]*, Ulrike Exner[1], Neil S. Mancktelow[2], and Djordje Grujic[3]
[1]Department for Geodynamics and Sedimentology, University of Vienna, 1090 Vienna, Austria
[2]Geological Institute, ETH Zurich, 8092 Zurich, Switzerland
[3]Department of Earth Sciences, Dalhousie University, Halifax, Nova Scotia B3H 4R2, Canada

ABSTRACT

Analog modeling of geological processes, such as folding instabilities or the behavior of inclusions in a matrix, often employs a linear simple-shear rig. In theory, a homogeneous plane-strain flow is prescribed at the boundaries of such deformation rigs but, in practice, the resulting internal deformation of the analog material (commonly paraffin wax or silicone putties) often deviates strongly from the intended homogeneous strain field. This can easily lead to misinterpretation of such analog experiments. We present a numerical finite-element approach to quantify the influence of imperfect simple-shear boundary conditions on the internal deformation of a homogeneous viscous analog material. The results demonstrate that imperfect boundary conditions in the vorticity-normal plane can cause the heterogeneous strain observed in some analog experiments. However, in other experiments, the analog material lies on top of a weak lubricating material or is sandwiched between two such materials. These layers lead to a viscous drag force acting on the analog material, resulting in imperfect simple-shear boundary conditions in the third dimension. For this experimental configuration, the numerical results show that the lubricating layers are responsible for the heterogeneous strain observed in analog models. The resulting errors in internal strain can be as high as 100%, and these difficult-to-avoid boundary effects must be considered when interpreting analog simple-shear experiments.

INTRODUCTION

Pure and simple shear are useful end-member descriptions of the two-dimensional (2-D) deformation of rocks, and represent practical geometries that can be attained in analog model experiments. Sufficiently accurate boundary conditions are obtained for pure-shear experiments, provided that friction between the analog material and the deformation apparatus is adequately reduced by lubrication (e.g., Mancktelow, 1988a). However, the results are less satisfactory for simple shear, where the opposite is desired, namely an effective transfer of shear stress at the model boundaries parallel to the shear direction. A range of linear simple-shear rigs has been developed (Cobbold and Quinquis, 1980; Price and Torok, 1989; Ildefonse et al., 1992; Ildefonse and Mancktelow, 1993; Piazolo et al., 2001; Sengupta and Koyi, 2001), all of which show boundary effects to some degree, resulting in a heterogeneous strain distribution within the models. This paper presents a numerical analysis of the three-dimensional (3-D) boundary effects that can occur in linear simple-shear rigs. Based on these results, we can critically assess the potential influence of boundary effects in many previous studies and provide suggestions for future improvements in rig design.

ANALOG MODELS

For clarity in describing both the analog rigs and the numerical models, it is necessary to establish a consistent nomenclature and coordinate system, which is defined in Table 1 and depicted in Figure 1. All boundaries are named after the coordinate axis perpendicular to this boundary in the undeformed state.

Design of Analog Simple-Shear Rigs

Linear shear machines vary in the details of their construction, but all have the same general characteristics. Simple-shear flow is imposed on the analog material via the walls of the deformation apparatus. Most commonly, the apparatus is arranged such that the vorticity vector of the simple-shear deformation is parallel to the gravity vector. This setup allows observation of the experiment from above and minimizes the effects of gravity. For example, in the simple-shear rig installed at the ETH Zurich (Fig. 1; Ildefonse and Mancktelow, 1993), the two x-boundaries together with the lower z-boundary consist of a stack of U-shaped metal plates. The y-boundaries are roughened by small sprockets to minimize slip of the analog material, which is especially important for strongly self-lubricating paraffin wax (Mancktelow, 1988a). This apparatus allows simple-shear strain up to $\gamma_{ext} \approx 3.7$ while maintaining parallel, non-rotating and non-stretching y-boundaries and rotating and stretching x-boundaries. Other analog machines have somewhat different designs but are based on the same fundamental principles of imposing simple-shear boundary conditions at the x- and y-boundaries (see Price and Torok, 1989; Ildefonse et al., 1992; Marques and Coelho, 2001; Piazolo et al., 2001; Mandal et al., 2005).

Boundary Effects in Analog Simple-Shear Rigs

In theory, a simple-shear apparatus should create a homogeneous isochoric plane-strain flow within the model. However, in practice, the internal deformation of the analog material often deviates strongly from the intended homogeneous strain field (Fig. 1; see also Price and Torok, 1989; Ildefonse and Mancktelow, 1993; Sengupta and Koyi, 2001; Bons et al., 2004). This is particularly undesirable if the results are used for precise quantification of the angular relationships between passive or active markers or for determining the orientation of inclusions. Generally, three types of strain heterogeneities occur to varying degrees in published examples of simple-shear experiments (and commonly all three occur together in a single experiment). These are: (1) bending of marker lines adjacent to the x-boundaries, generally rotating synthetically with the externally applied sense of rotation (Fig. 1; Price and Torok, 1989; Ildefonse

TABLE 1. DEFINITION OF THE COORDINATE SYSTEM, NOMENCLATURE OF THE BOUNDARIES, AND DEFINITIONS OF TERMS RELATED TO SIMPLE SHEAR DEFORMATION

| Term	Definition
x-coordinate	Parallel to the shear direction vector
y-coordinate	Perpendicular to the shear plane
z-coordinate	Parallel to the vorticity vector, which points in the negative z-direction
x-boundaries	Rotating and stretching boundaries initially perpendicular to the x-coordinate
y-boundaries	Translating boundaries perpendicular to the y-coordinate and parallel to the shear plane
z-boundaries	Perpendicular to the z-coordinate and to the vorticity vector
Shear direction	Parallel to the x-coordinate, pointing in the positive x-direction
Shear plane	Plane containing the shear direction vector and the vorticity vector
Vorticity-normal plane	Plane perpendicular to the vorticity vector (view plane in all figures in this paper)
$\dot{\gamma}_{ext}$ (and γ_{ext})	Shear strain rate (and resulting finite shear strain) externally applied at the boundaries
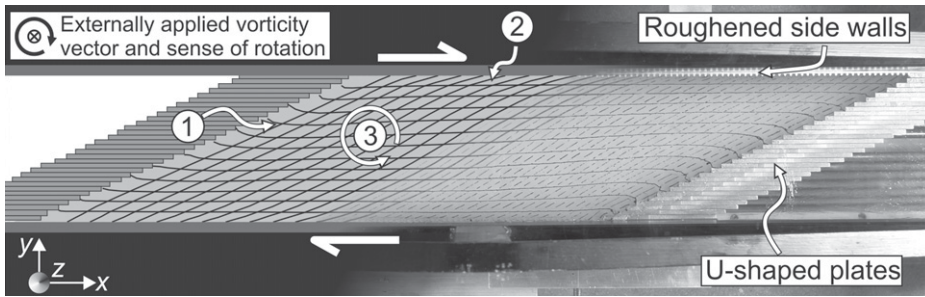
Figure 1. Photograph at γ_{ext} = 2.2 of analog simple-shear experiment using paraffin wax overlain by a schematic sketch of the same experiment (initial model dimensions: L_x = 29 cm, L_y = 12 cm, and L_z = 7.5 cm). Coordinate system used in this paper is shown in lower-left corner; the sense of shear leads to a vorticity vector pointing in the negative *z*-direction away from observer. Numbers refer to the characteristic types of heterogeneous strain described in text.

and Mancktelow, 1993; Grujic and Mancktelow, 1995; Sengupta and Koyi, 2001); (2) bending of marker lines adjacent to the *y*-boundaries, which can be either synthetic (Fig. 1; Ildefonse and Mancktelow, 1993) or antithetic to the externally applied sense of rotation (Price and Torok, 1989; Sengupta and Koyi, 2001); and (3) antithetic counter-rotation of marker lines in the model center, indicating a perturbation in vorticity opposite to that externally applied (Fig. 1; Grujic and Mancktelow, 1995).

NUMERICAL STUDY

To identify the cause of the observed deviations from perfect homogeneous simple shear, we developed a numerical finite-element model of a simple-shear experiment using an incompressible Newtonian viscous material. Because simple shear, by definition, is the description of a 2-D deformation, we apply a numerical code that simulates 2-D plane-strain deformation. The code (described in detail and successfully benchmarked in Frehner and Schmalholz, 2006) employs a Lagrangian numerical grid with nine-node quadrilateral elements, a mixed velocity-pressure-penalty formulation, and an Uzawa iteration to enforce incompressibility. The so-called natural boundary conditions, which arise by partially integrating the strong form of the governing equations to derive the weak form, provide full control over the imposed boundary conditions, something that is often difficult to attain with other numerical methods or in analog experiments.

Variations in the *x*- and *y*-Boundary Conditions

As a first approach, we ignore all effects of the *z*-boundaries and concentrate only on the vorticity-normal plane. In this plane, we define perfect simple-shear boundary conditions in terms of four separate constraints, illustrated in Figure 2A. These are: (1) $v_x = \dot{\gamma}_{ext} y$ at the *y*-boundaries; (2) $v_x = \dot{\gamma}_{ext} y$ at the *x*-boundaries; (3) $v_y = 0$ at the *y*-boundaries; and (4) $v_y = 0$

at the *x*-boundaries, where v_x and v_y are the velocity components in the *x*- and *y*-directions, respectively, and $\dot{\gamma}_{ext}$ is the externally applied shear strain rate (i.e., $\dot{\gamma}_{ext} = \partial_y v_x$). Only the combination of all four constraints leads to an internal homogeneous simple-shear deformation. Because it is difficult to fully control the boundary conditions in an analog experiment, any of these four constraints, or a combination of them, could be imperfect. Figures 2B–2E show the effects of four different combinations of imperfect boundary conditions on the internal distribution of the second invariant of finite strain (ε_{II}, or effective strain),

$$\varepsilon_{II} = \frac{1}{2}\sqrt{\left(\partial_x u_x - \partial_y u_y\right)^2 + \left(\partial_y u_x - \partial_x u_y\right)^2}, \quad (1)$$

where u_x and u_y are the two components of the 2-D finite displacement vector field. The applied external shear strain is γ_{ext} = 0.5 ($\gamma_{ext} = \partial_y u_x$). The effective strain for perfect homogeneous simple shear would be $\varepsilon_{II} = \frac{1}{2}\gamma_{ext}$ everywhere in the model. However, all four models show enhanced effective strains in the model centers and reduced effective strains toward the edges compared to homogeneous simple shear. Close to the *x*-boundaries, passive marker lines show the same synthetic sense of bending as in analog experiments. Close to the *y*-boundaries, the bending of passive marker lines is antithetic against the sense of shear, as observed in some (but not all) analog models (Price and Torok, 1989; Sengupta and Koyi, 2001). Antithetic counter-rotation in the center occurs in three of the imperfect-boundary-condition models. In all four models, the area for which the effective strain deviates by less than 10% from perfect simple shear is relatively small (<44%) and these areas of lowest error do not correspond to the model centers, but are more variably distributed. These results for models with imperfect boundary conditions in the vorticity-normal plane can explain the boundary effects observed in rigs where the *x*- and *y*-boundaries were lubricated (Price and Torok, 1989) or where the analog material was not very adherent (Sengupta and Koyi, 2001). However, they cannot explain the heterogeneous strain pattern observed in analog experiments such as shown in Figure 1.

Variations in *z*-Boundary Conditions

Real analog experiments are 3-D and often rest on a lubricating layer or are sandwiched between two such layers. These lubricating layers are also sheared during experiments and exert viscous drag forces on the analog material. Therefore, they yield imperfect boundary conditions at the *z*-boundaries. In 2-D, this effect can be approximated with a velocity-
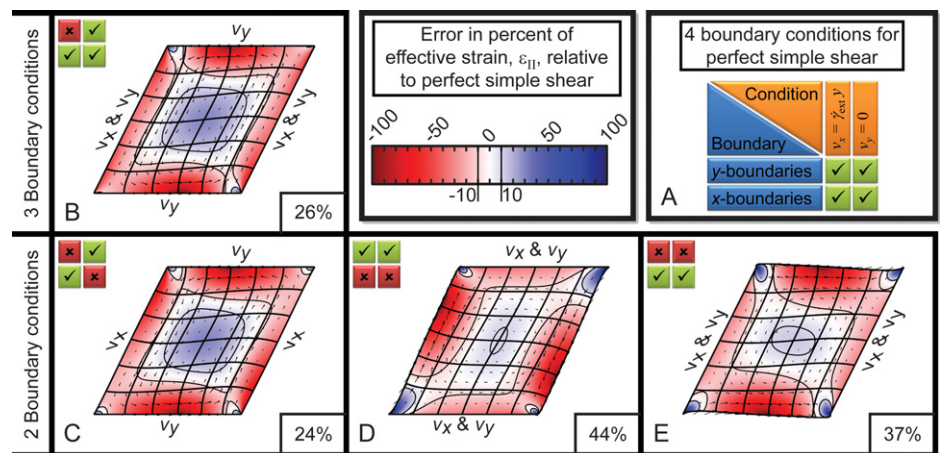

Figure 2. Numerically deformed homogeneous square subjected to simple shear with an applied shear strain of γ_{ext} = 0.5. A: Table listing the four boundary conditions necessary for perfect simple shear. B: Result of a model run with three of the four boundary conditions applied. C–E: Results of model runs with two of the four boundary conditions applied. Thick black lines are passive marker lines. Numbers in lower-right corners of B–E represent the area of models with an absolute error in ε_{II} (effective strain) smaller than 10%. Arrows represent the scaled finite perturbation displacement.

dependent viscous drag force in the force-balance equation:

$$\begin{Bmatrix} \partial_x \sigma_{xx} + \partial_y \sigma_{xy} \\ \partial_x \sigma_{xy} + \partial_y \sigma_{yy} \end{Bmatrix} = \frac{2\eta_{eff}}{hL_y} \begin{Bmatrix} v_x \\ v_y \end{Bmatrix}, \qquad (2)$$

where the spatial derivatives of the stress components are on the left-hand side and the velocity-dependent viscous drag forces in the x- and y-directions are on the right-hand side. In Equation 2, η_{eff} is the effective viscosity of the lubricating layer acting on the analog material, and h and L_y are the thickness in the z-direction and the width in the y-direction of the lubricating layer, respectively. Setting the right-hand side to zero results in the standard 2-D force-balance equation for slow, gravity-free deformation that was used in the previous section.

Figure 3 shows three snapshots of progressive simple-shear deformation of a homogeneous square model. The applied viscous drag force (Equation 2) corresponds to a deforming lubricating layer at the z-boundaries. Perfect simple-shear boundary conditions (i.e., all four constraints of Fig. 2A) are applied at the x- and y-boundaries. Hence, the strain heterogeneities in this numerical simulation are exclusively caused by the viscous drag boundary conditions at the z-boundaries. Both the second invariant of finite strain, ε_{II}, and the finite spin (ω_{xy}, or rigid body rotation) are plotted. The finite spin is given by

$$\omega_{xy} = \tfrac{1}{2}\left(\partial_y u_x - \partial_x u_y \right), \qquad (3)$$

with positive values for clockwise rotation, and $\omega_{xy} = \frac{1}{2}\gamma_{ext}$ throughout the model for perfect homogeneous simple shear. In Figure 3 both the finite spin, ω_{xy}, and the effective strain, ε_{II}, deviate strongly from homogeneous simple shear. The effective strain in the model center is almost equal to the externally applied value (<10% error), but is lower close to the x-boundaries and higher close to the y-boundaries. This leads to a synthetic sense of bending of the passive marker lines close to both the x- and y-boundaries. This feature is also present in analog models with a lubricated z-boundary (Fig. 1). The finite spin in the model center is much lower (>53% error), and toward the x- and y-boundaries much higher than that externally applied (Fig. 3). This leads to a counter-rotation similar to that observed in analog models. Between 41% and 47% of the model area shows a deviation of effective strain smaller than 10%, and this area covers the model center. However, only 15%–22% of the model area shows a deviation of finite spin smaller than 10%, and this area does not correspond to the model center but is distributed around it.

DISCUSSION

Analog laboratories have taken great effort to apply boundary conditions at the x- and y-boundaries as close to simple shear as possible, but commonly use a viscous lubricating layer at the z-boundaries. Our numerical simulations clearly show that the viscous drag force exerted by lubricating layers at the z-boundaries induces a heterogeneous strain pattern identical to that observed in many analog models. It is therefore desirable to minimize this drag force. However, few analog laboratories have designed their simple-shear rigs to specifically optimize the z-boundary conditions. Those designed and built at the Hans Ramberg Tectonic Laboratory (HRTL) in Uppsala, Sweden (Ildefonse et al., 1992; Sengupta and Koyi, 2001), and the ETH Zurich, Switzerland (Fig. 1; Ildefonse and Mancktelow, 1993), used a stack of thin parallel metal plates at the lower z-boundary, which, for thin enough plates, is a reasonable approximation to simple-shear boundary conditions on this boundary, as reflected in the good results for weak adhesive materials with a free upper surface (Ildefonse et al., 1992). However, experiments with paraffin wax require a glass plate to confine the upper boundary and result in very marked boundary effects (Fig. 1; Ildefonse and Mancktelow, 1993; Grujic and Mancktelow, 1995). The effect is almost certainly also present in other confined simple-shear experiments or in experiments using a lubricating layer at the base, but often no passive markers are drawn on the experimental upper surface (e.g., Marques and Coelho, 2001; Mandal et al., 2005), and potential boundary effects cannot be assessed.

Researchers are aware of possible boundary effects in their simple-shear rigs (e.g., Wood et al., 1979; Budhu, 1984) and therefore usually focus only on the center of the models. Our numerical simulations show that, depending on the apparatus design, the error in effective strain in the model center is relatively small. However, there can still be a large error in rotation (Fig. 3). In other words, angles between passive markers are still a good measure of the internal strain, but angles with respect to an external reference line are markedly in error. For example, many studies have investigated the rotation of a rigid inclusion in a simple-shear rig (Ildefonse et al., 1992; Mandal et al., 2005). Usually, the angle between the long axis of the inclusion and the y-boundaries is measured to provide a proxy for rotation. Such measurements can be influenced by the counter-rotation induced by boundary effects. The rotation rate of strongly elongated inclusions is very low when their long axis is subparallel to the y-boundaries and may be balanced or even exceeded by the counter-rotation developed due to boundary effects.

One way to overcome the problem of strongly heterogeneous strain is to increase the aspect ratio (L_x:L_y) of the modeling box. To test this, we numerically deformed a rectangle with an aspect ratio of 3:1. All other parameters are the same as in Figure 3. After a shear strain of $\gamma_{ext} = 0.5$ (Fig. 4), both the finite spin and the
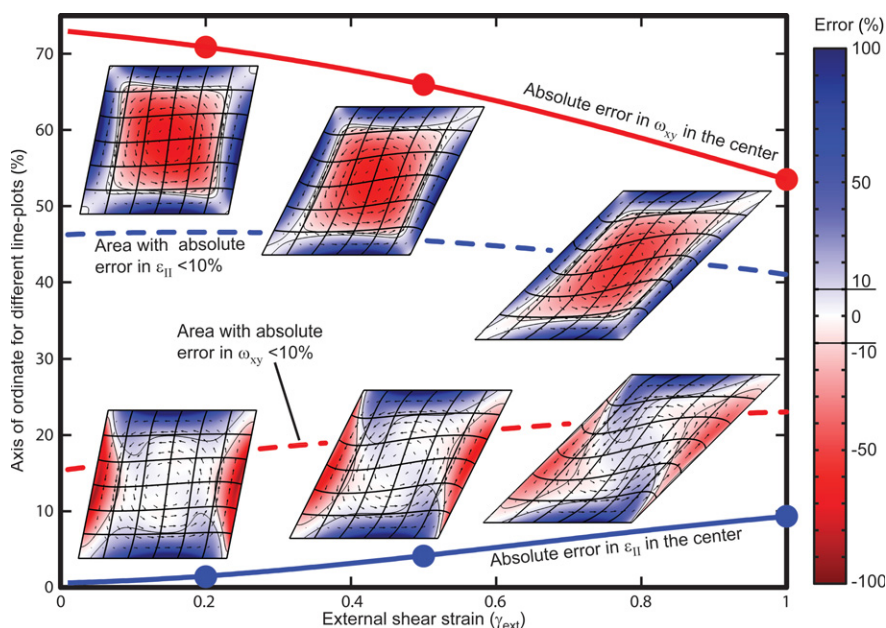

Figure 3. Numerically deformed homogeneous square subjected to simple shear with increasing applied shear strain and perfect simple-shear boundary conditions at *x*- and *y*-boundaries but viscous drag boundary conditions at *z*-boundaries (Equation 2). Colors represent ε_{II} (effective strain) in lower insets and ω_{xy} (rigid body rotation) in upper insets, respectively, both plotted as the percent error relative to perfect simple shear. Thick black lines are passive marker lines. Arrows represent the scaled finite perturbation displacement. Large dots indicate where the inset figures are plotted. Model parameters (see text): L_y:h = 2000:1 and η:η_{eff} = 100:1 (η is viscosity of analog medium).
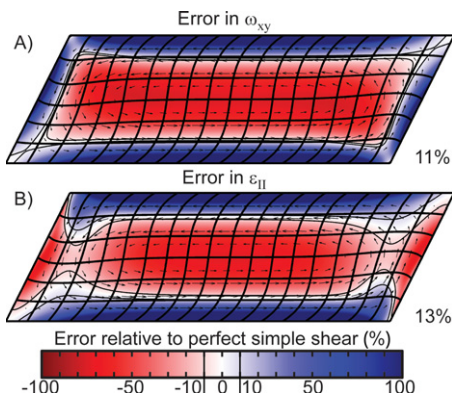
Figure 4. Numerically deformed homogeneous rectangle (initial aspect ratio L_x:L_y = 3:1) subjected to simple shear with an applied shear strain of γ_{ext} = 0.5. Boundary conditions and model parameters are identical to those of Figure 3. Thick black lines are passive marker lines. Arrows represent the scaled finite perturbation displacement. Numbers in lower-right corners represent the area of model with an absolute error in ω_{xy} (rigid body rotation) and ε_{II} (effective strain) smaller than 10%, respectively.

effective strain deviate strongly from perfect simple shear. The increased aspect ratio does not reduce the boundary effects. However, one advantage of a higher aspect ratio is the larger area in the model center with almost uniform effective strain, which undergoes simple shear but at a slower rate. In analog models, this area can be used as the investigation zone, but only if the effective strain in this area is well determined, because it is smaller than the value $\frac{1}{2}\gamma_{ext}$ expected for homogeneous simple shear. This can be achieved by modern experiment observation techniques, such as particle imaging velocimetry (Adam et al., 2005).

To study first-order effects, the chosen numerical model employs an incompressible Newtonian viscous rheology. For some analog materials, such as Polydimethylsiloxane (PDMS), this is a valid assumption (ten Grotenhuis et al., 2002); for others, such as paraffin wax (Mancktelow, 1988b), it is not, because of their power-law viscous rheology. However, the general conclusions of this paper will not change for a power-law viscous rheology. On the contrary, power-law viscous materials localize the deformation more than linear viscous materials, and the boundary effects, which represent a heterogeneous localization of deformation, will be even stronger.

Despite the sometimes strong boundary effects in analog experiments, laboratory data are valuable for understanding fundamental geomechanical concepts. Such concepts may specifically include the effects of boundary conditions. For example, Cotton and Koyi (2000) investigated the effects of frictional and ductile

substrates on the development of accretionary wedges. However, in such models, the frictional or viscous drag boundary conditions are deliberately set, whereas in the simple-shear rigs discussed in this paper they are unintentional. Ultimately, numerical and analog models should be compared, because not only analog models, but also numerical models, have their limitations, especially for more complex applications.

CONCLUSIONS

Similar heterogeneous strain patterns occur to various degrees in all analog experiments conducted in simple-shear deformation rigs. Our numerical simulations identify two potential causes of these heterogeneous strain patterns: (1) imperfect simple-shear boundary conditions at the z-boundaries as a result of viscous drag forces exerted by lubricating layers, and (2) imperfect simple-shear boundary conditions at the x- and/or y-boundaries. An increase in the aspect ratio of the modeling box does not reduce the boundary effects. Our numerical investigations prompt the following suggestions to workers conducting analog experiments.

(1) The z-boundaries should be left free or lubricated with a very low viscosity material and/or designed in such a way that proper simple-shear boundary conditions can be applied.

(2) Before modeling a heterogeneous medium (e.g., a rigid inclusion), a calibration model with the same boundary conditions should be performed using a homogeneous medium to quantify the boundary effects.

(3) The effective strain and rotation should generally be quantified within the model using passive marker lines and/or particle image velocimetry.

REFERENCES CITED

Adam, J., Urai, J.L., Wieneke, B., Oncken, O., Pfeiffer, K., Kukowski, N., Lohrmann, J., Hoth, S., van der Zee, W., and Schmatz, J., 2005, Shear localisation and strain distribution during tectonic faulting—New insights from granular-flow experiments and high-resolution optical image correlation techniques: Journal of Structural Geology, v. 27, p. 283–301, doi:10.1016/j.jsg.2004.08.008.

Bons, P.D., Druguet, E., Hamann, I., Carreras, J., and Passchier, C.W., 2004, Apparent boudinage in dykes: Journal of Structural Geology, v. 26, p. 625–636, doi:10.1016/j.jsg.2003.11.009.

Budhu, M., 1984, Nonuniformities imposed by simple shear apparatus: Canadian Geotechnical Journal, v. 21, p. 125–137, doi:10.1139/t84-010.

Cobbold, P.R., and Quinquis, H., 1980, Development of sheath folds in shear regimes: Journal of Structural Geology, v. 2, p. 119–126, doi:10.1016/0191-8141(80)90041-3.

Cotton, J.T., and Koyi, H.A., 2000, Modeling of thrust fronts above ductile and frictional detachments: Application to structures in the Salt Range and Potwar Plateau, Pakistan: Geological Society of America Bulletin, v. 112, p. 351–363, doi:10.1130/0016-7606(2000)112<351: MOTFAD>2.0.CO;2.

Frehner, M., and Schmalholz, S.M., 2006, Numerical simulations of parasitic folds in multilayers: Journal of Structural Geology, v. 28, p. 1647–1657, doi:10.1016/j.jsg.2006.05.008.

Grujic, D., and Mancktelow, N.S., 1995, Folds with axes parallel to the extension direction: An experimental study: Journal of Structural Geology, v. 17, p. 279–291, doi:10.1016/0191-8141(94)E0048-4.

Ildefonse, B., and Mancktelow, N.S., 1993, Deformation around rigid particles: The influence of slip at the particle/matrix interface: Tectonophysics, v. 221, p. 345–359, doi:10.1016/0040-1951(93)90166-H.

Ildefonse, B., Sokoutis, D., and Mancktelow, N.S., 1992, Mechanical interactions between rigid particles in a deforming ductile matrix. Analogue experiments in simple shear flow: Journal of Structural Geology, v. 14, p. 1253–1266, doi:10.1016/0191-8141(92)90074-7.

Mancktelow, N.S., 1988a, An automated machine for pure shear deformation of analogue materials in plane strain: Journal of Structural Geology, v. 10, p. 101–108, doi:10.1016/0191-8141(88)90132-0.

Mancktelow, N.S., 1988b, The rheology of paraffin wax and its usefulness as an analogue for rocks: Bulletin of the Geological Institutions of the University of Uppsala, new series, v. 14, p. 181–193.

Mandal, N., Samanta, S.K., Bhattacharyya, G., and Chakraborty, C., 2005, Rotation behaviour of rigid inclusions in multiple association: Insights from experimental and theoretical models: Journal of Structural Geology, v. 27, p. 679–692, doi:10.1016/j.jsg.2004.11.007.

Marques, F.O., and Coelho, S., 2001, Rotation of rigid elliptical cylinders in viscous simple shear flow: Analogue experiments: Journal of Structural Geology, v. 23, p. 609–617, doi:10.1016/S0191-8141(00)00135-8.

Piazolo, S., ten Gotenhuis, S.M., and Passchier, C.W., 2001, New apparatus for controlled general flow modeling of analog material, in Koyi, H.A., and Mancktelow, N., eds., Tectonic modeling: A volume in honor of Hans Ramberg: Geological Society of America Memoir 193, p. 235–244, doi:10.1130/0-8137-1193-2.235.

Price, G.P., and Torok, P.A., 1989, A new simple shear deformation apparatus for rocks and solids: Tectonophysics, v. 158, p. 291–309, doi:10.1016/0040-1951(89)90329-6.

Sengupta, S., and Koyi, H.A., 2001, Modifications of early lineations during later folding in simple shear, in Koyi, H.A., and Mancktelow, N., eds., Tectonic modeling: A volume in honor of Hans Ramberg: Geological Society of America Memoir 193, p. 51–68, doi:10.1130/0-8137-1193-2.51.

ten Grotenhuis, S.M., Piazolo, S., Pakula, T., Passchier, C.W., and Bons, P.D., 2002, Are polymers suitable rock analogs?: Tectonophysics, v. 350, p. 35–47, doi:10.1016/S0040-1951(02)00080-X.

Wood, D.M., Drescher, A., and Budhu, M., 1979, On the determination of stress state in the simple shear apparatus: Geotechnical Testing Journal, v. 2, p. 211–221, doi:10.1520/GTJ10460J.